

THE INFRARED PROPERTIES OF SUBMILLIMETER GALAXIES: CLUES FROM ULTRA-DEEP 70 μ m IMAGING

MINH T. HUYNH

Spitzer Science Center, MC220-6, California Institute of Technology, Pasadena CA 91125, USA. mhuynh@ipac.caltech.edu

ALEXANDRA POPE

Department of Physics and Astronomy, University of British Columbia, Vancouver, BC, V6T 1Z1, Canada

DAVID T. FRAYER

Spitzer Science Center, MC220-6, California Institute of Technology, Pasadena CA 91125, USA

DOUGLAS SCOTT

Department of Physics and Astronomy, University of British Columbia, Vancouver, BC, V6T 1Z1, Canada

Draft version June 12, 2018

ABSTRACT

We present 70 μ m properties of submillimeter galaxies (SMGs) in the Great Observatories Origins Deep Survey (GOODS) North field. Out of thirty submillimeter galaxies ($S_{850} > 2$ mJy) in the central GOODS-N region, we find two with secure 70 μ m detections. These are the first 70 μ m detections of SMGs. One of the matched SMGs is at $z \sim 0.5$ and has S_{70}/S_{850} and S_{70}/S_{24} ratios consistent with a cool galaxy. The second SMG ($z = 1.2$) has infrared-submm colors which indicate it is more actively forming stars. We examine the average 70 μ m properties of the SMGs by performing a stacking analysis, which also allows us to estimate that $S_{850} > 2$ mJy SMGs contribute $9 \pm 3\%$ of the 70 μ m background light. The S_{850}/S_{70} colors of the SMG population as a whole is best fit by cool galaxies, and because of the redshifting effects these constraints are mainly on the lower z sub-sample. We fit Spectral Energy Distributions (SEDs) to the far-infrared data points of the two detected SMGs and the average low redshift SMG ($z_{\text{median}} = 1.4$). We find that the average low- z SMG has a cooler dust temperature than local ultraluminous infrared galaxies (ULIRGs) of similar luminosity and an SED which is best fit by scaled up versions of normal spiral galaxies. The average low- z SMG is found to have a typical dust temperature $T = 21\text{--}33$ K and infrared luminosity $L_{8\text{--}1000\mu\text{m}} = 8.0 \times 10^{11} L_{\odot}$. We estimate the AGN contribution to the total infrared luminosity of low- z SMGs is less than 23%.

Subject headings: galaxies: formation — galaxies: evolution — galaxies: starburst — submillimeter

1. INTRODUCTION

Deep submillimeter surveys provide a probe of galaxies which is almost independent of luminosity for a wide redshift range $1 < z < 5$, because of the negative K-correction in the infrared (e.g. Blain et al. 2002). The Submillimeter Common User Bolometer Array (SCUBA; Holland et al. 1999) and Max-Planck Millimeter Bolometer (MAMBO, Kreysa et al. 1998) have now discovered several hundred submillimeter galaxies (SMGs: e.g. Smail et al. 1997, Hughes et al. 1998, Barger et al. 1998, Borys et al. 2002, Chapman et al. 2002, Webb et al. 2003, Greve et al. 2004, Pope et al. 2005, Coppin et al. 2006). Our knowledge of SMGs has been hampered by the large beamsizes of the submm telescopes, which makes it difficult to identify counterparts in the optical and near-infrared. For example, in the Great Observatories Origins Deep Survey (GOODS) North field there are typically ~ 10 *Hubble Space Telescope* (*HST*) Advanced Camera for Surveys (ACS) optical galaxies within a single SCUBA 15 arcsec beam.

Deep radio surveys have proven to be one of the best ways to identify the counterparts to SMGs (e.g. Ivison et al. 2000, Barger et al. 2000, Pope et al. 2006). The star formation processes that heat the dust

responsible for the submm light also produce radio emission, as evidenced by the well known far-infrared–radio correlation. Taking advantage of this, SMGs have been matched to radio sources, which have much better positional accuracy, and the optical/near-IR counterparts can then be found after the radio identification has been made. This is possible because the density of sources in the deepest radio images is much less than that of optical galaxies, so the probability of a chance coincidence is lower.

The current knowledge of SMGs is biased towards the radio identified sources. The SMGs have a median redshift of about 2.2 and bolometric infrared (IR) luminosities $L_{\text{IR}} > 10^{12} L_{\odot}$ (Chapman et al. 2004, 2005). The optically identified SMGs are faint optically, ($i_{775} \gtrsim 22$), and red ($i_{775} - K_s \simeq 2.3$ in AB magnitudes), with about 30% having colors consistent with Extremely Red Objects (EROs, Pope et al. 2005). Thus SMGs are thought to be high redshift, dusty analogs of local ultraluminous infrared galaxies (ULIRGs).

The spectral energy distributions (SEDs) of SMGs have traditionally been fit with local ULIRGs as templates, and in particular Arp220 (e.g. Barger et al. 2000), which has an effective dust temperature of about 42–

47 K (Klaas et al. 1997, Dunne et al. 2000). Chapman et al. (2005) found a typical dust temperature of 36 ± 7 K and a median $L_{\text{IR}} = 8.5 \times 10^{12} L_{\odot}$ for their SMG sample. This is cooler than local ULIRGs, which have an average dust temperature of 43 ± 6 K (based on the Dunne et al. 2000 sample). The Far-IR BACKground (FIRBACK) study of $170 \mu\text{m}$ selected galaxies found two ULIRGs between $0.5 < z < 1$ which have SEDs cooler and less luminous than Arp220 (Sajina et al. 2006). A $350 \mu\text{m}$ study of radio-detected SMGs found temperatures of 35 ± 3 K (Kovacs et al. 2006). Using the $24 \mu\text{m}$ imaging from the *Spitzer* Legacy Project GOODS, Pope et al. (2006) securely identify 60% of SMGs in this field in the mid-infrared (MIR), and have tentative counterparts for another 34%. It was found that the observed MIR–submm–radio SED of the SMGs peak at longer wavelengths than local ULIRGs and are best fit by models with temperatures of about 30 K (Pope et al. 2006). There is thus an emerging picture that SMGs are cooler than previously thought.

Dust temperature affects the inferred IR luminosity, and hence star formation rate (SFR), that is derived for these galaxies. Studies of SMGs have often assumed dust temperatures of 40 K (see Blain et al. 2002). A drop from 40 K to 35 K in temperature decreases the IR luminosity by about a factor of two. Better knowledge of the temperature of SMGs is thus crucial for more accurate luminosity estimates.

The advent of the *Spitzer Space Telescope* makes it possible to study the MIR and FIR properties of SMGs in detail for the first time. At the median SMG redshift of $z \sim 2$, PAH and silicate features fall into the rest-frame wavelength of the $24 \mu\text{m}$ band. This can make it difficult to determine the total infrared luminosities and to fit model SEDs well to the FIR, which does not always correlate with the MIR. The $70 \mu\text{m}$ band of the Multiband Imaging Photometer for *Spitzer* (MIPS) instrument is not affected by PAH or silicate features for redshifts less than about 3, while the $160 \mu\text{m}$ band is not affected at all. Moreover, these MIPS bands are closer to the FIR peak than the MIR data points used in previous studies. The longer wavelength MIPS bands should therefore be extremely useful for studying SMGs. The sensitivities and confusion limits at $70 \mu\text{m}$ make this feasible, but difficult, and hence only the deepest MIPS data are likely to lead to SMG detections.

In this paper we present a study of the FIR properties and SEDs of submm galaxies using the deepest 70 and $160 \mu\text{m}$ data available for the GOODS-N field. In particular, we use the 70 and $160 \mu\text{m}$ data to check if the SEDs of distant SMGs are consistent with those of local ULIRGs.

We assume a Hubble constant of $71 \text{ km s}^{-1} \text{ Mpc}^{-1}$, together with matter and cosmological constant density parameters of $\Omega_{\text{M}} = 0.27$ and $\Omega_{\Lambda} = 0.73$ in this paper. We also use the notation S_{70} , S_{850} , $S_{1.4}$ etc. throughout for the flux densities at $850 \mu\text{m}$, $70 \mu\text{m}$ and 1.4 GHz.

2. THE SUBMILLIMETER SAMPLE

The SCUBA ‘super-map’ of GOODS-N contains 35 robust $850 \mu\text{m}$ detections. Details of the data reduction and source extraction can be found in Borys et al. (2003) and Pope et al. (2005). This submm image contains all publicly available SCUBA mapping data in

this field taken up until 2004. Although $450 \mu\text{m}$ data were also taken, they unfortunately have essentially no constraining power. Of the 35 SCUBA sources, 33 have likely radio and/or *Spitzer* counterparts using the Very Large Array (VLA), InfraRed Array Camera (IRAC) and MIPS $24 \mu\text{m}$ data in GOODS-N (see Pope et al. 2006). Thirty of these SCUBA galaxies are within the ultra-deep $70 \mu\text{m}$ image area. SCUBA sources with low signal-to-noise ratios (SNRs) may have true flux densities which are boosted by a factor which depends on the source brightness and the local noise in the SCUBA map, and can be estimated if the source counts are known (see e.g. Coppin et al. 2005). Therefore in this study we use the deboosted $850 \mu\text{m}$ flux densities given in Pope et al. (2006).

3. SPITZER 70 AND $160 \mu\text{m}$ OBSERVATIONS

The MIPS $70 \mu\text{m}$ observations were carried out during Cycle 1 of the General Observer program (*Spitzer* program ID 3325, Frayer et al. 2006). The inner $10' \times 10'$ of GOODS-N was mapped to a depth of 10.6 ksec. The data were taken in the small-field photometry mode of MIPS with 10-second Data Collection Events (DCEs). Each Astronomical Observation Request (AOR) consisted of an 8-position cluster map, and the observations were completed with 12 AORs in total. In addition to our GO data, we used the MIPS Guaranteed Time Observers (GTO) data (program ID 81, Dole et al. 2004). These GTO data have an integration time of 600 sec.

The raw data were processed off-line using the Germanium Reprocessing Tools (GERT, version S13.1), following the algorithms derived by the MIPS team (Gordon et al. 2005). Instrumental artifacts in the Basic Calibrated Data (BCDs) were removed using the filtering techniques adopted for the extragalactic First Look Survey (xFLS, Frayer et al. 2006a). The data were calibrated assuming an absolute flux calibration factor of 702 MJy sr^{-1} per MIPS- $70 \mu\text{m}$ unit for stellar SEDs. The flux densities were multiplied by 1.09 to apply a galactic SED color correction. This assumes a power law SED of the form $f_{\nu} \propto \nu^{\alpha}$ and $\alpha = -1$, but the color corrections are similar for $\alpha = 0$ to -3 . A more detailed discussion of the data reduction can be found in Frayer et al. (2006b).

The final image achieves a sensitivity of $\sim 0.6 \text{ mJy rms}$ and we have cataloged 101 sources (over 120 arcmin^2) with $S_{70} > 2.3 \text{ mJy}$ ($\text{SNR} > 3\sigma$). We catalog a region slightly larger than the area of deepest coverage to include some relatively bright $70 \mu\text{m}$ sources and improve statistics. The source counts are presented in Frayer et al. (2006b) and a full catalog will be presented in Huynh et al. (in preparation). The $70 \mu\text{m}$ image has a beam size of $18''.5$ FWHM, and in the presence of Gaussian noise the 1σ positional error of sources is of the order $0.5 \theta_{\text{FWHM}}/\text{SNR}$, i.e. $3''$ for the faintest sources.

The $160 \mu\text{m}$ observations of the GOODS-N region were taken as part of the MIPS GTO program in 2004. These data were taken in the scan mode of MIPS and we applied the standard filtering techniques to the $160 \mu\text{m}$ BCDs similar to what was used for the xFLS (Frayer et al. 2006a). The data were calibrated using a factor of 44.7 MJy sr^{-1} per MIPS- $160 \mu\text{m}$ unit. The $160 \mu\text{m}$ data have an effective integration time of 120 seconds and the $160 \mu\text{m}$ image reaches a sensitivity of $\sim 15 \text{ mJy rms}$. A multiplication of 1.04 was applied to the $160 \mu\text{m}$ flux den-

sities to color correct for galaxy SEDs. We also note that the $160\ \mu\text{m}$ light leak from $1 - 1.6\ \mu\text{m}$ is not a problem for this data because there are no blue sources with $m_J \gtrsim 5.5$ in the field.

4. IDENTIFICATIONS AT 70 AND $160\ \mu\text{m}$

The negative K-correction at submillimeter wavelengths means that SMGs are detectable in deep SCUBA images over a wide redshift range, $1 < z < 5$ (e.g. Blain et al. 2002). However, at 70 and $160\ \mu\text{m}$, the K-correction does not compensate for the distance dimming, and the flux density of a galaxy with a given intrinsic luminosity drops steeply as a function of redshift (e.g. Lagache et al. 2005). This is reflected in the high median redshifts of the SMGs ($z \simeq 2.0$, Pope et al. 2006) compared to the $70\ \mu\text{m}$ sources ($z \simeq 0.5$, Huynh et al. in preparation). Hence the SMG and $70\ \mu\text{m}$ samples are unlikely to have much overlap, and we only expect to detect the low redshift SMGs in deep $70\ \mu\text{m}$ imaging.

We examined the $70\ \mu\text{m}$ image for counterparts to the SCUBA sources. To do this the $70\ \mu\text{m}$ catalogue positions were compared to IRAC positions of the SCUBA counterparts (Pope et al. 2006), searching within $10''$ of each submm counterpart. This search radius was chosen in order to take into account the typical positional uncertainties of low SNR $70\ \mu\text{m}$ and SCUBA sources added in quadrature.

This procedure uncovered two secure identifications of SMGs at $70\ \mu\text{m}$, GN26 and GN13 (following the naming convention of Pope et al. 2005). These sources have $70\ \mu\text{m}$ SNRs of 12 and 8, respectively, and hence $70\ \mu\text{m}$ positional uncertainties of about $1''.3$ and $1''.5$ (including the *Spitzer* $1''$ pointing uncertainty). The positional offset of the $70\ \mu\text{m}$ source relative to the IRAC position is 0.6 and 0.3 arcsec for GN26 and GN13, respectively, which is well within the positional uncertainty. The probability that one or more $70\ \mu\text{m}$ sources lies randomly within a distance θ of a SCUBA counterpart is:

$$P = 1 - \exp(-\pi n \theta^2), \quad (1)$$

given a surface density n of $70\ \mu\text{m}$ sources (often called the P -statistic, e.g. Downes et al. 1986). Hence the probability of any $70\ \mu\text{m}$ source lying within $1''$ of a SCUBA counterpart is 0.07%, using the $70\ \mu\text{m}$ source density of 101 sources over $120\ \text{arcmin}^2$, and hence the $70\ \mu\text{m}$ matches to GN13 and GN26 are likely to be real.

Two more SMGs (GN12 and GN32) have a nearby $70\ \mu\text{m}$ source at distances of $4.7''$ and $9.5''$, respectively. The $70\ \mu\text{m}$ sources near GN12 and GN32 have IRAC and $24\ \mu\text{m}$ counterparts which do not match the identifications for the SCUBA source (Pope et al. 2006). Although it is likely that some fraction of the $70\ \mu\text{m}$ flux density is associated with the submm galaxy, it is difficult to determine this fraction because of the other $24\ \mu\text{m}$ sources in the vicinity. Using Equation (1), the random probability that 2/30 SCUBA sources have a $70\ \mu\text{m}$ source within a distance of $10''$ can be determined to be 28%. This is consistent with the $70\ \mu\text{m}$ sources near GN12 and GN32 being random matches.

At $160\ \mu\text{m}$ the only SMG detected is GN26. The beamsize at $160\ \mu\text{m}$ is $40''$, so $70\ \mu\text{m}$ and/or SCUBA sources which are close together may be blended into one $160\ \mu\text{m}$ source. Examination of the $70\ \mu\text{m}$ MIPS image suggests that the $160\ \mu\text{m}$ flux density of GN26

has some contribution from another $70\ \mu\text{m}$ source (at $z = 0.46$) not associated with GN26. We therefore deblended GN26 with a double Gaussian fit, fixing positions to the IRAC counterparts of the two $70\ \mu\text{m}$ sources which contribute to the $160\ \mu\text{m}$ flux density. We find that GN26 has $S_{160} = 110 \pm 27\ \text{mJy}$, which is 60% of the flux density of the $160\ \mu\text{m}$ complex. The uncertainty at $160\ \mu\text{m}$ is conservatively estimated to be 25%, taking into account absolute calibration, fitting errors, and deblending issues. We also examined the SED of the source near GN26 to check the accuracy of the deblending. The S_{70}/S_{160} ratio of the second source at $z = 0.46$ is well fit by the quiescently star-forming galaxy SED templates of Dale & Helou (2002), so the deblending at $160\ \mu\text{m}$ seems reasonable.

The multi-wavelength properties of the two SMGs which are detected at $70\ \mu\text{m}$ (Figure 1 and Table 1) are described in detail in Pope et al. (2006). As expected, both sources (GN26 and GN13) are in the low redshift tail of the submm redshift distribution. Furthermore, we notice that these two sources are among the faintest at $850\ \mu\text{m}$ in the submm sample (both have $S_{850} < 2.5\ \text{mJy}$) and therefore they are not typical of the full submm sample presented in Pope et al. (2006) or indeed other samples of SMGs. GN13 and GN26 have $70\ \mu\text{m}$ flux densities of 6.5 and 13.9 mJy, respectively, while the full $70\ \mu\text{m}$ catalog has a median flux density of 5 mJy. About 80% of the $70\ \mu\text{m}$ sources have spectroscopic redshifts, and the median redshift of these sources is $z = 0.46$ (Huynh et al. in preparation). Thus the $70\ \mu\text{m}$ counterpart to GN13 is typical of the full $70\ \mu\text{m}$ sample, but GN26 is unusual in that it has a bright $70\ \mu\text{m}$ counterpart, and is one of only seven $70\ \mu\text{m}$ sources in our sample currently confirmed to be at $z > 1$.

5. STACKING ANALYSIS

We performed a stacking analysis to derive an average $70\ \mu\text{m}$ flux density for the SMG population in the GOODS-N field. To begin with, we stacked the *Spitzer* data at the positions of all SMGs, including sources with $70\ \mu\text{m}$ matches or with coincident flux. For each SMG a square image $132''$ on a side (approximately 7 MIPS beams) was extracted. We rotated each image by 90° with respect to the previous one before co-adding to remove any large-scale background effects. The median level of the individual extracted images was subtracted to remove any small scale offsets and yield better background removal. Flux densities were determined using an aperture of $12''$ radius, and we applied an aperture correction of 2.0, which was calculated empirically from bright sources in the image. The aperture photometry was done after the background was subtracted from the stacked images, and the results were verified by making measurements with different size sky annuli.

To estimate the expected scatter, offset stacked images were generated by randomly choosing a position in the $70\ \mu\text{m}$ image for each stacked source. Five hundred such random stacks were generated, and the uncertainty in the stacked flux density is taken to be the standard deviation of these 500 measured values.

The average $70\ \mu\text{m}$ flux density ($\langle S_{70} \rangle$) for all 30 SMGs is $2.00 \pm 0.48\ \text{mJy}$, and hence the stacked signal is detected at over 4σ . The contribution from SMGs to the Extragalactic Background Light (EBL) at $70\ \mu\text{m}$ can be

estimated from this stacked signal by multiplying by the appropriate source density. Assuming the SMG integrated source count of $2506 \pm 406 \text{ deg}^{-2}$ for $S_{850} > 2 \text{ mJy}$ (Coppin et al. 2006), we estimate the contribution to the $70 \mu\text{m}$ EBL from SMGs to be $0.016 \pm 0.005 \text{ MJy sr}^{-1}$. From an extrapolation of the source counts Frayer et al. (2006b) find that the total $70 \mu\text{m}$ EBL is 0.18 MJy sr^{-1} , so SMGs ($S_{850} > 2 \text{ mJy}$) make up about $9 \pm 3\%$ of the $70 \mu\text{m}$ EBL.

The $70 \mu\text{m}$ stacked signal from all 30 SMGs is dominated by the 4 low redshift sources with coincident $70 \mu\text{m}$ flux density. To determine the average properties of the SMGs *not* detected at $70 \mu\text{m}$, which is more representative of the general SMG population, we also stacked the 26 sources without coincident $70 \mu\text{m}$ flux density. This time we stacked the residual $70 \mu\text{m}$ image, which was obtained by removing all sources brighter than 3σ at $70 \mu\text{m}$. Sources were removed by subtracting their fitted point spread functions from the image. The residual image was used to obtain a better signal to noise ratio in the stacked image and in the measured stacked flux density. For these 26 sources we find $\langle S_{70} \rangle = 0.70 \pm 0.27 \text{ mJy}$, and so this stacked signal has an SNR of about 3.

To test whether the majority of the stacked $70 \mu\text{m}$ flux density is from the lower redshift SMGs, we also looked at low and high redshift sub-samples. The low redshift sub-sample consists of 12 SMGs out of the 26 with $z < 2$, and the remaining 14 SMGs with $z \geq 2$ make up the high redshift sub-sample. For redshift completeness we included IRAC photometric redshifts from Pope et al. (2006) for 8/26 SMGs, and these all have $z \geq 1.8$ (and estimated accuracy of $\Delta z \leq 0.4$). The aperture flux density in the central region of the high redshift stack is $0.22 \pm 0.44 \text{ mJy}$, while for the low redshift stack it is more positive at $1.0 \pm 0.4 \text{ mJy}$. This is consistent with the idea that the majority of the flux density from the full sample is coming from the lower redshift sources, although the measurements are too noisy to make a definitive statement.

Similarly, we stacked the $160 \mu\text{m}$ image at all SMG positions, excluding the one detected source, GN26. There is no significant flux density in the stacked image and the 3σ upper limit is 13 mJy . A stack of the 12 low redshift SMGs gives a 3σ upper limit at $160 \mu\text{m}$ of 22 mJy .

To study the FIR properties of SMGs we could use the average flux densities of the full sample of SMGs. However, the stacked $70 \mu\text{m}$ flux density from the separate high- and low- z sub-samples clearly show that most of the signal is coming from $z < 2$ sources (as expected from the K-correction). We therefore limit our analyses to the average properties of the low- z sub-sample in the following sections.

6. INFRARED COLORS

The average IR colors, S_{70}/S_{850} and S_{70}/S_{24} , are shown in Figure 2 as a function of redshift. GN26, at $z \sim 1.5$ is consistent with a more active Dale & Helou (2002, hereafter DH02) model, with dust intensity index $\gamma = 1.5$, whereas GN13 has cooler colors, corresponding to $\gamma = 2.5$. In the DH02 models γ defines the amount of dust as a function of heating intensity (Dale et al. 2001):

$$dM(U) \propto U^{-\gamma} dU,$$

where $M(U)$ is the dust mass heated by a radiation field of intensity U . These γ values span the range expected for infrared luminous galaxies – a low value around 1 implies a high contribution from photo-dissociation regions in an actively star-forming galaxy, while a significantly higher value represents the cirrus-dominated interstellar medium of a more quiescent or cooler galaxy.

The infrared colors of the average low- z SMG are consistent with $\gamma \simeq 2$ –2.5 DH02 SEDs. The average S_{70}/S_{850} ratio of SMGs from the stacking analysis indicates that the SMGs are relatively cool galaxies for their high IR luminosities, which is consistent with Pope et al. (2006). We also calculated upper limits to the S_{70}/S_{850} ratio for SMGs *not* detected individually at $70 \mu\text{m}$ (see Figure 2). The lower redshift SMGs are clearly inconsistent with lower values of γ . For the higher redshift sources we expect much lower S_{70}/S_{850} ratios, but with the current observational limits these sources can still be actively star-forming.

For GN13, Figure 2 shows that the S_{70}/S_{24} ratio is that of an actively star-forming galaxy, with $\gamma \simeq 1$ –1.5, while the S_{70}/S_{850} ratio indicates it is a cooler galaxy. This may be due to broad silicate absorption falling into the $24 \mu\text{m}$ band; the S_{70}/S_{24} ratio can be strongly affected by PAH features and silicate absorption, which are not fully accounted for in the models.

We find that the colors of GN26 are consistent with DH02 models with $\gamma = 1$ and $z \simeq 1$ –2 (Figure 3). The colors of GN13 place it at $z = 1$ –2 if a $\gamma = 1.5$ model is assumed (Figure 3). However, GN13 is at $z = 0.475$ and so this SMG has a warmer S_{70}/S_{24} ratio than that suggested by its S_{70}/S_{850} ratio, as mentioned earlier.

The average colors of low- z SMGs are also plotted in Figure 3. We find that the average IR colors are best represented with a DH02 model having $\gamma \simeq 2$ –2.5 at $z = 1$ –2. This is consistent with the median redshift of the low- z SMG sub-sample, and suggests the color-color plot can be used as a crude redshift indicator.

7. SPECTRAL ENERGY DISTRIBUTION

The FIR photometry at 70 and $160 \mu\text{m}$ provides valuable data points for constraining the FIR peak. Combined with the $850 \mu\text{m}$ observations, the photometry spans both sides of the peak. Previous estimates of the SED of SMGs have relied on extrapolating the MIR or radio to fit the FIR peak – at the redshifts of SMGs, the MIR can be affected by complex emission and absorption features, so this method may not be reliable.

We fit a variety of models to the data. These include four DH02 models with $\gamma = 1, 1.5, 2,$ and 2.5 , as well as the Chary & Elbaz (2001, hereafter CE01) SEDs, which are templates derived from ISOCAM, IRAS and SCUBA data of nearby galaxies. The CE01 models have luminosity dependent shapes, but since the local luminosity–temperature relation found for nearby galaxies may not hold for high- z SMGs (e.g. Pope et al. 2006), we fit CE01 models allowing them to scale arbitrarily in luminosity.

For GN13 and for the low- z SMG sub-sample, we constrain the fit with the 70 and $850 \mu\text{m}$ observations only, since they are not detected at $160 \mu\text{m}$ (although the $160 \mu\text{m}$ data provide a useful upper limit). For GN26, the $70, 160$ and $850 \mu\text{m}$ observations are all used to constrain the fit. We summarize the fitting results in Table 2, while Figures 4 and 5 show the best fit SEDs for GN13,

GN26, and the average low- z SMG. Fitting CE01 SEDs without allowing the luminosity to vary freely results in relatively poor fits, so we exclude these from the Table. This confirms the Pope et al. (2006) result that the local luminosity–temperature relationship does not hold for SMGs. For each best fit SED the total L_{IR} (between 8 and 1000 μm) was calculated and given in Table 2. Uncertainties in the luminosity were derived by scaling the best fit SED until the minimum χ^2 value exceeded the 68% ($\pm 1\sigma$) confidence interval.

The models provide good fits to the 70 and 850 μm data for GN13 and for the low- z average SMG, but they do not typically fit the 24 μm (observed) data point, although it has been shown that the 24 μm flux density can often be fit with additional extinction (Pope et al. 2006). The models do not provide a similarly good fit in the FIR for GN26; the 70 and 850 μm data points of GN26 are well fit, but the 160 μm measurement is underestimated by the models. Hence the luminosity for GN26 is probably higher than given by these models. Nevertheless, our derived IR luminosity for GN26 is 3 times greater than that estimated by Pope et al. (2006) from fitting SEDs to 24 μm , 850 μm and 1.4 GHz radio data. It is possible that there are further deblending issues at 160 μm for GN26 (even although we have already divided the total 160 μm flux density between the two 70 μm sources in the area). This demonstrates the power of 160 μm photometry in constraining the total infrared luminosity of galaxies, but shows that higher resolution is required to study such faint sources individually.

The SMGs have high luminosities, but their FIR spectral shape is different from local ULIRGs of the same luminosity. We find that the average low- z SMG has a total IR luminosity of about $8.0 \times 10^{11} L_{\odot}$. This is a factor $\simeq 2$ less than the median SMG luminosity found by Pope et al. (2006) and Chapman et al. (2005) for their SMGs with $z < 2$. The reason that our calculated SMG luminosities are low compared to previous results is because our best fit SEDs are cooler. The average SMG is best fit by a quiescent DH02 model with $\gamma \simeq 2.5$, or with CE01 SED templates of normal spiral galaxies scaled up by a factor $\simeq 300$, with a rest-frame peak at about 150 μm (i.e. $T \simeq 20$ K). Local ULIRGs of the same luminosity as the SMGs are therefore not the best spectral templates for this sample.

Several recent studies have relied on the MIR data (at 24 μm in particular) to derive luminosities and SED fits (e.g. Pérez-González et al. 2005, Le Floc’h et al. 2005). The 24 μm flux density was used in SED fitting of SMGs by Pope et al. (2006), who found that the typical SMG peaks at about 100 μm (corresponding to about 29 K). If the 24 μm data point is included in the fitting of GN13 along with the 70 and 850 μm data, we find the best fit DH02 SED peaks at shorter wavelength, corresponding to warmer dust temperatures, and the total IR luminosity is decreased by a factor of about 2. There is no significant difference in the CE01 fits to GN13 with and without the 24 μm data point. For GN26 we find the 24 μm data point makes no significant difference to the best fit DH02 SED, while the best fit CE01 model is slightly warmer and 3 times less luminous. The fit to the average SMG including the 24 μm data point is warmer than that with only the longer wavelength data, and the best fit DH02 and CE01 SEDs are about 2 times more

luminous. At the median redshift of the average low- z SMG, $\langle z \rangle = 1.4$, PAH and silicate features fall into into the 24 μm band, and our fit here is driven by these features in the model SEDs. The DH02 and CE01 SEDs certainly contain PAH features, but it is not clear whether SMGs at this redshift have strong or weak PAH features, if any. Therefore we would argue that the fit to the 850 and 70 μm flux densities alone gives a more reliable result for the average SMG total luminosity, at least for the moment, until we learn more about the MIR spectra of SMGs.

8. DUST TEMPERATURES AND MASSES

As a phenomenological alternative, we also adopt a modified blackbody SED model to fit the temperature of these SMGs. The SED is described by $f_{\nu} \propto \nu^{\beta} B_{\nu}$, where $B_{\nu}(\nu, T)$ is the blackbody function for dust of temperature T , and β is the dust emissivity index. The MIR is approximated as a power-law of the form $f_{\nu} \propto \nu^{-\alpha}$ and smoothly matches $\nu^{\beta} B_{\nu}$ at longer wavelengths (Blain et al. 2003). Although this simple phenomenological model cannot describe the full complex dust properties of a galaxy, it can provide a good description of the general behavior of the SED. The range of parameters we consider is $15 \text{ K} < T < 90 \text{ K}$ and $1 < \alpha < 4$, which is representative of galaxies ranging from normal spirals to AGN. We set $\beta \equiv 1.5$ for our model fits, which is the value found for dust in the galactic plane (Masi et al. 1995), and a typical value for well-studied nearby galaxies (Dunne et al. 2000).

We fit for T and α using the 70 μm and 850 μm data points for GN13 and the average low- z SMG, but also include the 160 μm detection for GN26. The results are summarized in Table 3. When fitting only two data points (and allowing the normalization to also be free) there is a strong degeneracy between α and T (which would be complete except for the boundaries of the parameter ranges) – so the fit parameters must be interpreted with caution. In the case of GN13, the full range of α is allowed by the 70 and 850 μm data, with low values of α corresponding to low values of T . Because of the additional 160 μm data point, the parameters are better constrained for GN26, with $T \simeq 45$ K and $\alpha \simeq 3.5$ being preferred.

For the average SMG, the 70 and 850 μm flux densities alone cannot break the T and α degeneracy – a very low temperature of 15 K is allowed for $\alpha \simeq 1.0$, while $T \simeq 33$ K for $\alpha \simeq 4.0$. In a sample of 73 radio-detected SMGs the average S_{450}/S_{850} ratio is measured to be 5.0 ± 2.3 (Chapman et al. 2005), while 15 SMGs from this same sample have been detected with SHARC-II (Kovacs et al. 2006) and they have an average S_{350}/S_{850} ratio of 4.0 ± 1.3 . We find that models with $\alpha < 1.6$ are inconsistent with these ratios. This implies that the allowed models for the average SMG have $21 \text{ K} < T < 33 \text{ K}$ and $1.6 < \alpha < 4.0$, where the low values of T require low α . This shows that the low- z SMGs have relatively cool dust temperatures.

The best fit dust temperatures of 21–33 K are consistent with those values previously derived for SMGs (e.g. Pope et al. 2006). Chapman et al. (2005) and Kovacs et al. (2006) suggested average temperatures close to the upper end of our acceptable range. This implies that the average low- z SMG in our sample has a

relatively steep mid-IR SED, since our model fits with $T \simeq 30$ K require $\alpha \simeq 3$. This suggests that the SMGs are star-forming galaxies, because large α implies cool mid-IR colors, which are inconsistent with AGN-dominated sources.

Assuming that the submm light is thermal emission from dust which is optically thin at $\lambda_{\text{rest}} \sim 200 \mu\text{m}$, with a single dust temperature T , the dust mass M_{d} is given by:

$$M_{\text{d}} = \frac{S_{850} D_{\text{L}}^2}{(1+z) \kappa_{\text{d}}(\nu_{\text{rest}}) B_{\nu}(\nu_{\text{rest}}, T)}, \quad (2)$$

(e.g. McMahon et al. 1994), where D_{L} is the cosmological luminosity distance at redshift z and the dust absorption coefficient κ is uncertain, even in the local Universe. We take a κ value of $0.077 \pm 0.030 \text{ m}^2 \text{ kg}^{-1}$ (Hughes et al. 1993), converting it to rest-frame frequency ν_{rest} with:

$$\kappa_{\text{d}}(\nu_{\text{rest}}) = 0.077 \left(\frac{\nu_{\text{rest}}}{350 \text{ GHz}} \right)^{\beta}. \quad (3)$$

Here we again assume that the dust emissivity index β is fixed at 1.5.

The range of allowable dust masses are calculated from the range of temperatures in Table 3. The dust mass calculated from Equation (2) is $1.0\text{--}1.6 \times 10^8 M_{\odot}$ and $2.2\text{--}2.5 \times 10^8 M_{\odot}$ for GN13 and GN26, respectively, while the dust mass found for the average low- z SMG is $1.1\text{--}2.6 \times 10^9 M_{\odot}$. This does not take into account the uncertainties in κ and S_{850} ; the dust mass uncertainty is about 50% when these are added in quadrature. These dust masses are consistent, within uncertainties, with the molecular gas mass derived from CO observations (e.g. Frayer et al. 1998, Frayer et al. 1999, Neri et al. 2003, Greve et al. 2005), assuming a typical galactic gas mass to dust mass ratio $M_{\text{g}}/M_{\text{d}} \simeq 100$ (e.g. Hildebrand 1983).

9. FIR–RADIO CORRELATION

Our sample can be used to test the FIR–radio correlation in submillimeter galaxies. The FIR–radio correlation is often expressed as (e.g. Yun et al. 2001):

$$q \equiv \log \left(\frac{\text{FIR}}{3.75 \times 10^{12} \text{ W m}^{-2}} \right) - \log \left(\frac{S_{1.4}}{\text{W m}^{-2} \text{ Hz}^{-1}} \right), \quad (4)$$

where ‘FIR’ here refers to the flux between 40 and 120 μm . The observed local value is $q = 2.34 \pm 0.3$ (Yun, Reddy and Condon 2001). We use the best fit DH02 models to derive the conversion from $L_{40\text{--}120}$ to $L_{8\text{--}1000}$, which is 2.0 and 1.6 for GN13 and GN26, respectively. Based on their L_{IR} (Table 2), we find q parameters of $2.5^{+0.3}_{-0.1}$ and $2.4^{+0.1}_{-0.1}$ for GN13 and GN26, respectively. These values are consistent with the local value of q , suggesting that these two sources follow the local FIR–radio correlation.

10. CONTRIBUTION FROM ACTIVE GALACTIC NUCLEI

As mentioned in Section 8, the inferred high values of α suggest that AGN do not dominate the bolometric luminosity in our sample of SMGs. To quantify the contribution of AGN to the infrared luminosity of SMGs, we adopt the simple modified blackbody approach as described in Section 8. For our AGN model we use $\beta = 1.5$,

$T = 90$ K, and $\alpha = 1.1$, as found for the xFLS AGN population (Frayer et al. 2006). We subtract this AGN component from the observed 70 and 850 μm flux densities of the average SMG, and then repeat the fitting procedure with the DH02 and CE01 models, increasing the AGN component until the best fit χ^2 value exceeds the previous minimum by 1σ . This allows us to estimate the maximum AGN contribution to the FIR luminosity, with the results shown in Figure 5.

It could be argued that the MIR waveband is the best discriminator of AGN, and therefore we should be focussing on the 24 μm data point (e.g. Sajina et al. 2005). However, we are here calculating the percentage contribution of AGN to the L_{IR} , which is dominated by the FIR peak, and the contribution from AGN emission in the MIR is only a very small proportion of the total IR luminosity.

For the average low- z SMG, an AGN which contributes up to 14% of the IR luminosity is allowed, using only the previous best fit CE01 SED model. If all CE01 models are used in the refitting, an AGN component of up to 23% contribution is allowed. Together these fitting procedures imply that the average (low- z sub-sample) SMG is dominated by a starburst. This is consistent with X-Ray studies which find that AGN contribute on average 10% to the infrared luminosity of SMGs (Alexander et al. 2005).

For the 70 μm detected SMGs, GN13 and GN26, we find that 32% and 21%, respectively, of the total IR luminosity can be attributed to an AGN from the same analysis applied to the best fit templates. However, if the whole suite of CE01 SEDs are used, a larger proportion of the IR luminosity can be subtracted off the observed data points, with lower luminosity CE01 models still fitting. This shows that with the current data a low luminosity starburst model from CE01 with an additional dominant AGN component is indistinguishable from a high luminosity CE01 ULIRG model, and that further photometry (or spectroscopy) is needed.

Another method to estimate the AGN contribution is to make use of the 24 μm data. Here, we consider the extreme case where all the 24 μm flux density is due to an AGN, and determine its contribution to the total IR luminosity. For GN13 and GN26 such an AGN would contribute 11% and 5%, respectively, to the total IR luminosity, assuming the $T = 90$ K, $\alpha = 1.1$ AGN model used above, and the CE01 best fit SEDs. For the average low- z SMG, 21% of the total IR luminosity could be attributed to an AGN in this extreme case. This again supports the hypothesis that SMGs are dominated by star formation processes.

11. CONCLUDING REMARKS

We have presented 70 μm properties of submillimeter galaxies in the GOODS-N field. Out of 30 SMGs (with $S_{850} > 1.7$ mJy) in the overlap region of this field, 2 are detected at relatively high significance in ultra-deep (~ 0.6 mJy rms) 70 μm imaging. Both of these detected SMGs lie at relatively low redshift. One SMG, GN26 at redshift $z = 1.2$, has infrared colors which indicate it is actively star forming. The second SMG, GN13 ($z = 0.47$) has infrared colors similar to normal spirals, but with a much higher luminosity. We confirm that these two SMGs detected at 70 μm follow the locally derived FIR–

radio correlation.

To determine the average properties of SMGs (most of which lie at $z > 2$ and are not detected individually at $70 \mu\text{m}$), we performed a stacking analysis and find that the average SMG has a $70 \mu\text{m}$ flux density of $0.70 \pm 0.27 \text{ mJy}$. Most of the $70 \mu\text{m}$ flux density is coming from the lower redshift SMGs however. We analysed the average properties of twelve SMGs with $z < 2$, which have a stacked $70 \mu\text{m}$ flux density of $1.0 \pm 0.4 \text{ mJy}$. From a stack of all 30 SMGs in the ultra-deep $70 \mu\text{m}$ image, we find that the contribution of SMGs (with $S_{850} > 2 \text{ mJy}$) to the total Extragalactic Background Light at $70 \mu\text{m}$ is $9 \pm 3\%$.

The average low- z SMG ($\langle z \rangle = 1.4$) has cool infrared colors and an FIR SED that is best fit by a scaled up (about $300\times$) normal spiral galaxy. We also found that an AGN contributes less than 23% of the total IR luminosity in SMGs.

We find that the average low- z SMG has an IR luminosity, L_{8-1000} , of $8.0(\pm 2.2) \times 10^{11} L_{\odot}$. The average low- z SMG therefore has a star formation rate of $135 \pm 35 M_{\odot} \text{ yr}^{-1}$, using the relationship between SFR and IR luminosity for starburst galaxies given by Kennicutt (1998). GN13 and GN26 have star-formation rates of 30 ± 10 and $800 \pm 270 M_{\odot} \text{ yr}^{-1}$, respectively. The median IR luminosity of $z < 2$ SMGs in Chapman et al. (2005) is twice the value we find for our average low- z SMG, suggesting that theirs may have been an overestimate, suffering from lack of FIR data.

The next generation submillimeter bolometer,

SCUBA-2, will come online in 2007 (Holland et al. 2006) and it is expected to yield a major improvement at $450 \mu\text{m}$, where it should reach a confusion limit of $\sim 1 \text{ mJy}$ (5σ). This depth is well-matched to that of deep *Spitzer* $70 \mu\text{m}$ imaging and should provide much more overlap than the $850 \mu\text{m}$ selected sources. In addition, SCUBA-2 will produce much larger samples of fainter $850 \mu\text{m}$ sources, much like the two $70 \mu\text{m}$ detected submm sources in this study, and therefore $70 \mu\text{m}$ data will be a valuable addition to understanding their SEDs. Also in the near future, the *Herschel Space Observatory* will produce confusion limited images across the wavelength range $75\text{--}500 \mu\text{m}$. *Herschel* will therefore enable detailed study of the far-IR SEDs of large samples of SMGs, which we have shown here to be feasible for a sub-set of SMGs using *Spitzer*.

We thank the anonymous referee for helpful comments that improved this paper. MTH would like to thank Anna Sajina for helpful discussions. AP and DS acknowledge support from the Natural Sciences and Engineering Research Council of Canada and the Canadian Space Agency. This work is based in part on observations made with the *Spitzer Space Telescope*, which is operated by the Jet Propulsion Laboratory, California Institute of Technology under a contract with NASA. Support for this work was provided by NASA through an award issued by JPL/Caltech.

REFERENCES

- Alexander, D. M., Bauer, F. E., Chapman, S. C., Smail, I., Blain, A. W., Brandt, W. N., & Ivison, R. J. 2005, *ApJ*, 632, 736
- Barger, A. J., Cowie, L. L., & Richards, E. A. 2000, *AJ*, 119, 2092
- Barger, A. J., Cowie, L. L., Sanders, D. B., Fulton, E., Taniguchi, Y., Sato, Y., Kawara, K., & Okuda, H. 1998, *Nature*, 394, 248
- Blain, A. W., Barnard, V. E., & Chapman, S. C. 2003, *MNRAS*, 338, 733
- Blain, A. W., Smail, I., Ivison, R. J., Kneib, J.-P., & Frayer, D. T. 2002, *Phys. Rep.*, 369, 111
- Borys, C., Chapman, S. C., Halpern, M., & Scott, D. 2002, *MNRAS*, 330, L63
- Chapman, S. C., Blain, A. W., Smail, I., & Ivison, R. J. 2005, *ApJ*, 622, 772
- Chapman, S. C., Lewis, G. F., Scott, D., Borys, C., & Richards, E. 2002, *ApJ*, 570, 557
- Chapman, S. C., Smail, I., Blain, A. W., & Ivison, R. J. 2004, *ApJ*, 614, 671
- Coppin, K., et al. 2006, *ArXiv Astrophysics e-prints*, astro-ph/0609039
- Coppin, K., Halpern, M., Scott, D., Borys, C., & Chapman, S. 2005, *MNRAS*, 357, 1022
- Dale, D. A., & Helou, G. 2002, *ApJ*, 576, 159
- Dale, D. A., Helou, G., Contursi, A., Silbermann, N. A., & Kolhatkar, S. 2001, *ApJ*, 549, 215
- Dole, H., et al. 2004, *ApJS*, 154, 87
- Downes, A. J. B., Peacock, J. A., Savage, A., & Carrie, D. R. 1986, *MNRAS*, 218, 31
- Dunne, L., Eales, S., Edmunds, M., Ivison, R., Alexander, P., & Clements, D. L. 2000, *MNRAS*, 315, 115
- Frayer, D. T., et al. 2006a, *AJ*, 131, 250
- Frayer, D. T., et al. 2006b, *ApJ*, 647, L9
- Frayer, D. T., et al. 1999, *ApJ*, 514, L13
- Frayer, D. T., Ivison, R. J., Scoville, N. Z., Yun, M., Evans, A. S., Smail, I., Blain, A. W., & Kneib, J.-P. 1998, *ApJ*, 506, L7
- Gordon, K. D., et al. 2005, *PASP*, 117, 503
- Greve, T. R., et al. 2005, *MNRAS*, 359, 1165
- Greve, T. R., Ivison, R. J., Bertoldi, F., Stevens, J. A., Dunlop, J. S., Lutz, D., & Carilli, C. L. 2004, *MNRAS*, 354, 779
- Hildebrand, R. H. 1983, *QJRAS*, 24, 267
- Holland, W., et al. 2006, in *Millimeter and Submillimeter Detectors and Instrumentation for Astronomy III*. Edited by Zmuidzinas, Jonas; Holland, Wayne S.; Withington, Stafford; Duncan, William D.. *Proceedings of the SPIE*, Volume 6275, pp. (2006).
- Holland, W. S., et al. 1999, *MNRAS*, 303, 659
- Hughes, D. H., Robson, E. I., Dunlop, J. S., & Gear, W. K. 1993, *MNRAS*, 263, 607
- Hughes, D. H., et al. 1998, *Nature*, 394, 241
- Ivison, R. J., Smail, I., Barger, A. J., Kneib, J.-P., Blain, A. W., Owen, F. N., Kerr, T. H., & Cowie, L. L. 2000, *MNRAS*, 315, 209
- Kennicutt, R. C. 1998, *ARA&A*, 36, 189
- Klaas, U., Haas, M., Heinrichsen, I., & Schulz, B. 1997, *A&A*, 325, L21
- Kreysa, E., et al. 1998, in *Proc. SPIE Vol. 3357*, p. 319-325, *Advanced Technology MMW, Radio, and Terahertz Telescopes*, Thomas G. Phillips; Ed., ed. T. G. Phillips, 319
- Lagache, G., Puget, J.-L., & Dole, H. 2005, *ARA&A*, 43, 727
- Le Floc'h, E., et al. 2005, *ApJ*, 632, 169
- Masi, S., et al. 1995, *ApJ*, 452, 253
- McMahon, R. G., Omont, A., Bergeron, J., Kreysa, E., & Haslam, C. G. T. 1994, *MNRAS*, 267, L9
- Neri, R., et al. 2003, *ApJ*, 597, L113
- Pérez-González, P. G., et al. 2005, *ApJ*, 630, 82
- Pope, A., Borys, C., Scott, D., Conzelice, C., Dickinson, M., & Mobasher, B. 2005, *MNRAS*, 358, 149
- Pope, A., et al. 2006, *MNRAS*, 370, 1185
- Sajina, A., Lacy, M., & Scott, D. 2005, *ApJ*, 621, 256
- Sajina, A., Scott, D., Dennefeld, M., Dole, H., Lacy, M., & Lagache, G. 2006, *MNRAS*, 370, 1185
- Smail, I., Ivison, R. J., & Blain, A. W. 1997, *ApJ*, 490, L5
- Webb, T. M., et al. 2003, *ApJ*, 587, 41
- Yun, M. S., Reddy, N. A., & Condon, J. J. 2001, *ApJ*, 554, 803

TABLE 1
SUMMARY OF THE PROPERTIES OF GN13, GN26 AND THE AVERAGE LOW- z SMG.

galaxy	RA J2000	Dec J2000	S_{24} (μ Jy)	S_{70} (mJy)	S_{160} (mJy)	S_{850} (mJy)	$S_{1.4}$ (μ Jy)	z
GN13	12 36 49.72	62 13 12.8	371.0 ± 10.4	6.5 ± 1.3	<43	1.9 ± 0.4	45.4 ± 5.4	0.475
GN26	12 36 34.51	62 12 40.9	446.0 ± 5.1	13.9 ± 1.8	110 ± 27	2.2 ± 0.8	194.3 ± 10.4	1.219
low- z SMG (12 sources)			258 ± 20	1.0 ± 0.4	<22	4.0 ± 1.4	<116	1.4

NOTE. — The 70 and 160 μ m flux densities include the absolute calibration error (of order 10%). The coordinates for GN13 and GN26 are IRAC positions (Pope et al. 2006). The redshift given for the low- z SMGs is the median for the sub-sample, and the S_{850} value given for the low- z sub-sample is the weighted average.

TABLE 2
SUMMARY OF THE BEST FIT SEDS AND THE CALCULATED TOTAL L_{IR} .

galaxy	best fit DH02	DH02 L_{IR} (L_{\odot})	lum scaled CE01 L_{IR} (L_{\odot})
GN13	$\gamma = 2.5$	$(2.5 \pm 0.3) \times 10^{11}$	$(1.8 \pm 0.2) \times 10^{11}$
GN26	$\gamma = 1.5$	$(4.5 \pm 0.7) \times 10^{12}$	$(5.0 \pm 0.7) \times 10^{12}$
low- z SMG (12 sources)	$\gamma = 2.5$	$(9.0 \pm 2.5) \times 10^{11}$	$(8.0 \pm 2.2) \times 10^{11}$

TABLE 3
ALLOWABLE MODEL PARAMETERS FOR A SIMPLE MODIFIED BLACKBODY SED.

galaxy	T (K)	α
GN13	34 – 50	1.0 – 4.0
GN26	44 – 48	3.0 – 4.0
low- z SMG (12 sources)	21 – 33	1.6 – 4.0

NOTE. — The range in T and α indicates the models which fit within the 1σ limit of the 70, 160 and 850 μ m observations. The dust emissivity parameter, β , is assumed to be 1.5.

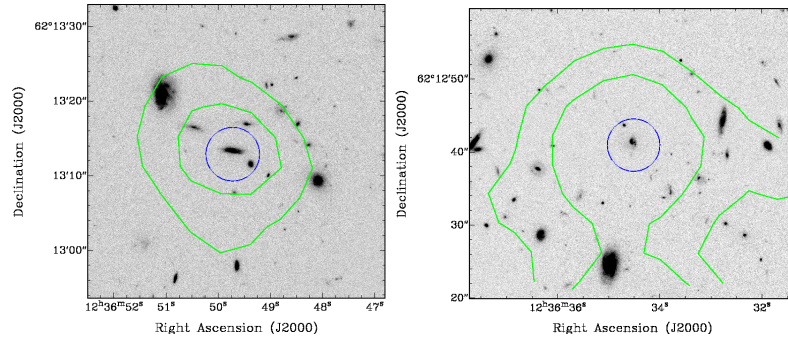


FIG. 1.— Greyscale *HST* ACS F606W images of GN13 (left panel) and GN26 (right panel). The contours show $70\ \mu\text{m}$ data, plotted at 3σ and 6σ levels. The circle indicates the Pope et al. (2006) IRAC counterpart to the SCUBA source. The images are $40'' \times 40''$ in size.

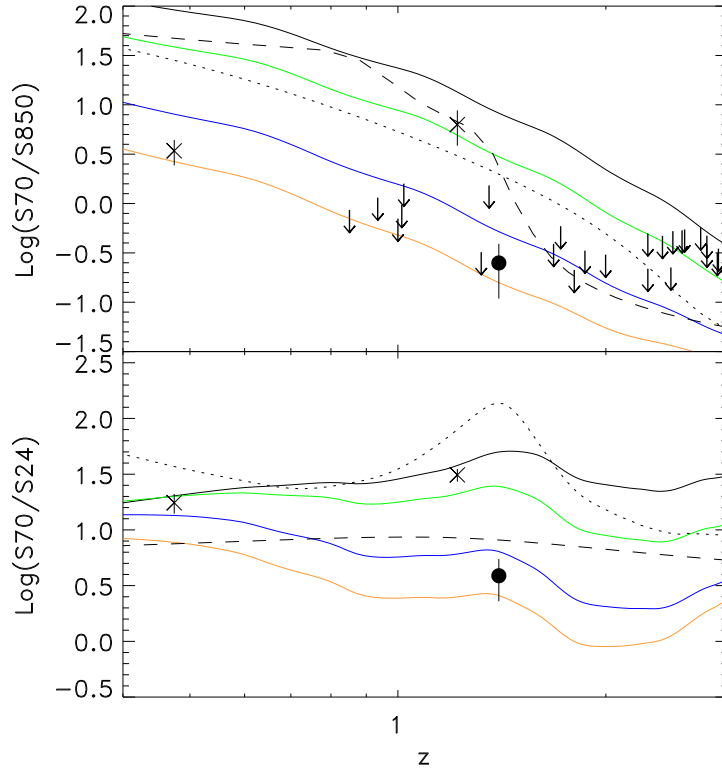


FIG. 2.— Top Panel: S_{70}/S_{850} colors of the DH02 models as a function of redshift. From top to bottom, the solid lines are $\gamma = 1, 1.5, 2,$ and 2.5 . The dotted line marks an Arp220 SED, while the dashed line is Mrk231. The crosses mark the SMGs GN13 and GN26, which are detected at $70\ \mu\text{m}$. Other SMGs are shown as 3σ upper limits. The filled circles denote the average ratios from the stacked analysis of the low- z sub-sample at $\langle z \rangle = 1.4$. Bottom Panel: S_{70}/S_{24} colors of the DH02 models. Lines and symbols are as for the top panel.

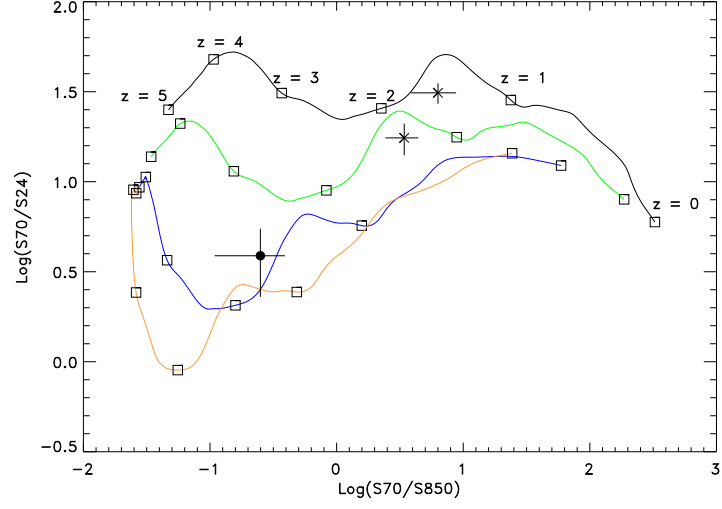


FIG. 3.— S_{70}/S_{24} versus S_{70}/S_{850} colors compared with the DH02 models. For each model the squares mark redshift 0, 1, 2, 3, 4, and 5, from right to left. The models from top to bottom are for $\gamma = 1, 1.5, 2,$ and 2.5 . The crosses mark the SMGs GN13 and GN26, which are detected at $70\ \mu\text{m}$. The filled circle marks the average for the low- z SMG sub-sample.

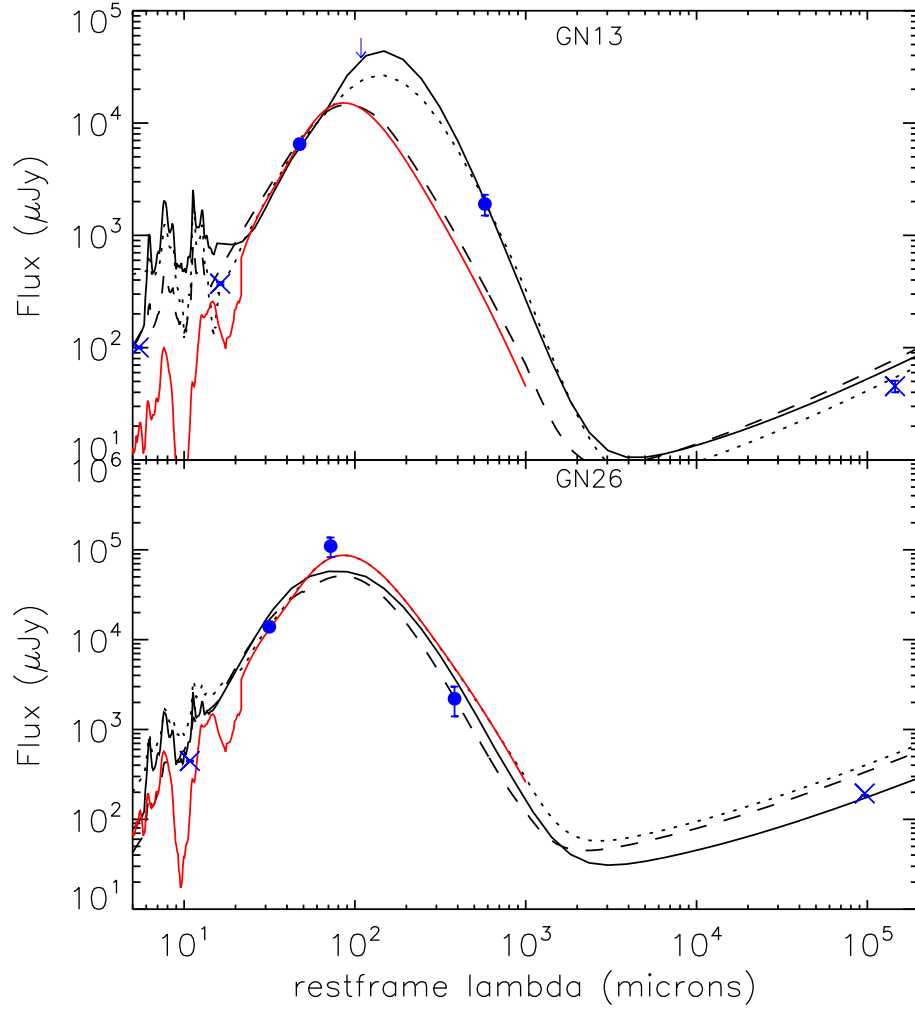


FIG. 4.— SEDs of GN13 and GN26. The observed *Spitzer* and SCUBA data are plotted at rest-frame wavelengths. The best fit DH02 model is plotted as a solid black line, while the dashed curve is the best fit CE01 luminosity dependent SED and the dotted line is the best fit CE01 SED with luminosity allowed to vary. The best fit Arp220 SED is also shown as the red solid line. The fits were constrained using only by the 70 and 850 μm data for GN13, and with the addition of the 160 μm data point for GN26.

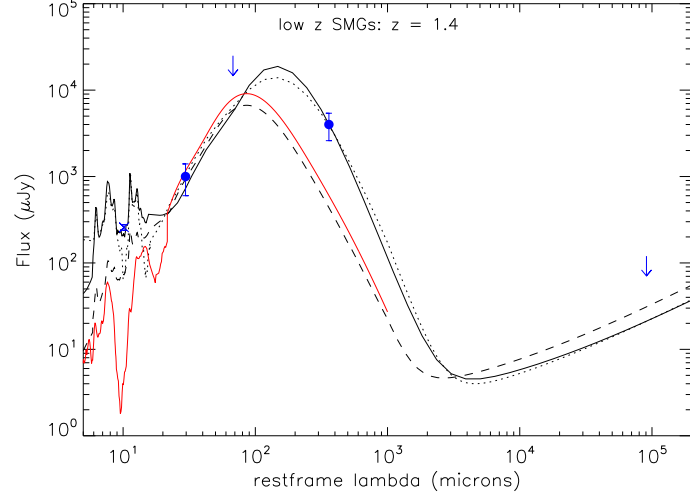


FIG. 5.— The SED of the average low- z SMG. The observed *Spitzer* and SCUBA data are plotted at rest-frame wavelengths and the curves are: best fit DH02 model (solid black line); best fit CE01 luminosity-dependent SED (dashed line); best fit CE01 SED with luminosity allowed to vary (dotted line); and best fit Arp220 SED (red solid line). The fits were constrained using the 70 and 850 μm data only, as described in the text.

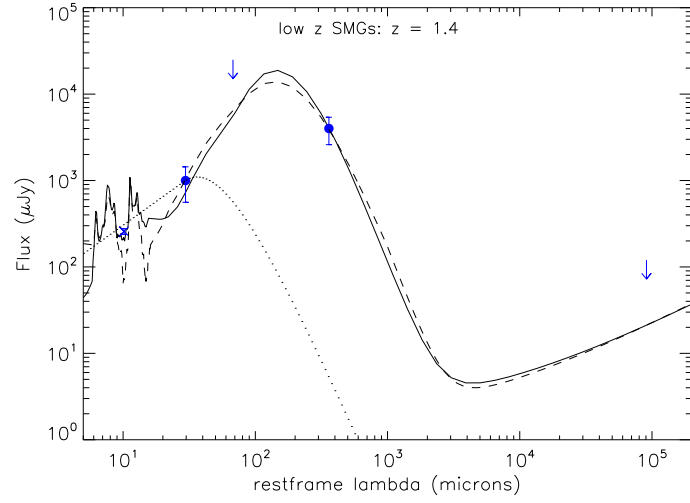


FIG. 6.— The best fit SEDs for the low- z SMG sub-sample. The solid line is the DH02 model and the dashed line is the best fit CE01 model (allowing the luminosity to float freely). The dotted line shows the AGN contribution allowed before all the CE01 models fail at the 1σ level. The symbols are as for Figure 5.